

A NEW DEFORMATION FAMILY OF SCHWARZ' D SURFACE

HAO CHEN AND MATTHIAS WEBER

ABSTRACT. We prove the existence of a new 2-parameter family $\mathfrak{o}\Delta$ of embedded triply periodic minimal surfaces of genus 3. The new surfaces share many properties with classical orthorhombic deformations of Schwarz' D surface, but also exotic in many ways. In particular, they do not belong to Meeks' 5-dimensional family. Nevertheless, $\mathfrak{o}\Delta$ meets classical deformations in a 1-parameter family on its boundary.

1. INTRODUCTION

This is the first of two papers dealing with new 2-dimensional families of embedded triply periodic minimal surfaces (TPMS) of genus three whose 1-dimensional “intersections” with the well-known Meeks family exhibit singularities in the moduli space of TPMS.

In the past three decades, the classification of complete, embedded minimal surfaces of finite topology in Euclidean space forms has largely been accomplished for the smallest reasonable genus ([MPR98, LHM01, PRT05, MR05, PT07]). In all these cases, the moduli space of these surfaces has been found to be a smooth manifold.

In the case of triply periodic minimal surfaces, no such classification has been found. For the lowest possible genus 3, there is an explicit 5-dimensional smooth family described by Meeks [Mee90] that contains most of the then known examples, with the notable exception of Schwarz' H surfaces and Schoen's Gyroid. Work of Traizet [Tra08] implies that the H-surfaces belong to a second 5-dimensional family for which no explicit description is known. Our other paper will explore that family.

In this paper, we construct a new 2-dimensional family of embedded triply periodic minimal surfaces of genus 3 that does not belong to the Meeks family but whose closure meets the Meeks family in a 1-dimensional subset. More specifically, the surfaces in this subset are *bifurcation instances* in the sense that, with the same deformation of their lattices, they may deform either within a classical 2-parameter Meeks family, or into a new 2-parameter non-Meeks family. Existence of the latter is the focus of this paper.

In fact, all these surfaces can be seen as orthorhombic deformations of Schwarz' D surface. Hence we begin with a description of the classical orthorhombic deformations of D, which all belong to the Meeks family.

Consider an embedded minimal surface S inside an axis parallel box $[-A, A] \times [-B, B] \times [0, 1]$ that solves the following partially free boundary problem: S satisfies free boundary condition on the vertical planes $x = \pm A$ and $y = \pm B$, and fixed (Plateau) boundary condition on the horizontal segments $\{(x, 0, 0) \mid -A \leq x \leq A\}$ and $\{(0, y, 1) \mid -B \leq y \leq B\}$, and the intersection of ∂S with each face of the

Date: July 28, 2020.

2010 Mathematics Subject Classification. Primary 53A10.

Key words and phrases. Triply periodic minimal surfaces.

H. Chen is supported by Individual Research Grant from Deutsche Forschungsgemeinschaft within the project “Defects in Triply Periodic Minimal Surfaces”, Projektnummer 398759432.

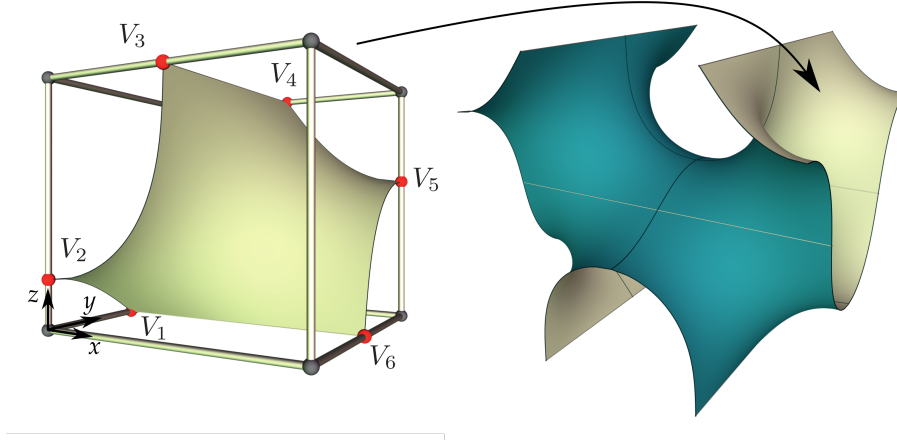


FIGURE 1.1. Fundamental Piece and Translational Fundamental Piece

box has at most one component. S is therefore a right-angled embedded minimal hexagon. See Figure 1.1 (left) for an example.

Because the two horizontal segments are in the middle of the top and bottom faces of the box, rotations about them and reflections in the lateral faces of the box extend S to an embedded TPMS $\tilde{\Sigma}$. More specifically, $\tilde{\Sigma}$ is invariant under the lattice Λ spanned by $(4A, 0, 0)$, $(0, 4B, 0)$ and $(2A, 2B, 2)$. In the 3-torus \mathbb{R}^3/Λ , $\Sigma = \tilde{\Sigma}/\Lambda$ is a compact surface of genus 3. In Figure 1.1 (right) we show a translational fundamental domain of $\tilde{\Sigma}$ nicely presented in a box. It consists of eight copies of S .

Remark 1.1. For crystallographers, the orthorhombic lattice spanned by $(4A, 0, 0)$, $(0, 4B, 0)$ and $(0, 0, 4)$ is probably more convenient. This is responsible for the letter “o” in our naming. The quotient of $\tilde{\Sigma}$ by this lattice is a double cover of Σ , hence of genus 5.

We use \mathcal{D} to denote the set of all TPMS obtained in this way.

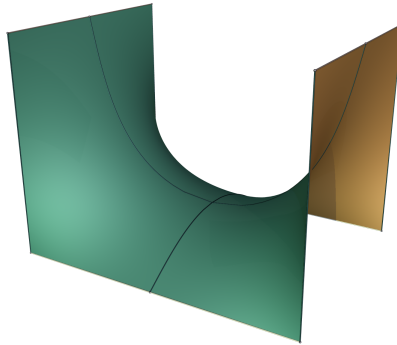


FIGURE 1.2. Plateau construction of oD surfaces

A well-known family of surfaces in \mathcal{D} is the tD family of H. A. Schwarz, which is a tetragonal deformation family of his famous D surface. They are obtained as described above with $A = B$ and S containing the vertical segment $\{(0, 0, z) \mid 0 \leq z \leq 1\}$. The same construction also applies when $A \neq B$, yielding an orthorhombic deformation of Schwarz’ D surface, known as oDb in the literature to distinguish

from another orthorhombic deformation family oDa ; see [FK89, FH92]. In this paper, we simply use oD in place of oDb .

An alternative (better known) construction of an oD surface starts with a box of the same dimensions and then solves the Plateau problem for a polygonal contour running along edges of the box, as shown in Figure 1.2. The Plateau solution is unique and therefore shares the symmetries of the contour. In particular, it has reflectional symmetries by vertical planes. To relate with the previous construction, just divide the minimal surface into quarts by cutting along these planes, then extend one of the quarts by rotating it about its vertical edge.

The main result of this paper is to confirm the existence of another 2-parameter family in \mathcal{D} .

Theorem 1.2. *There exists a second 2-parameter continuous family $\text{o}\Delta$ in \mathcal{D} , lacking the vertical straight line of the oD surfaces.*

The $\text{o}\Delta$ family, well hidden in the radiance of the famous oD family, is understandably unexpected. The second author confesses his complete bafflement and initial disbelief when the first author provided him with evidence of $\text{o}\Delta$. In Figure 1.3 we compare oD and $\text{o}\Delta$ surfaces with the same lattice (the surfaces in this figure actually have tetragonal lattices, hence belong to tD and $\text{t}\Delta$ subfamilies that we will discuss in Section 6.)

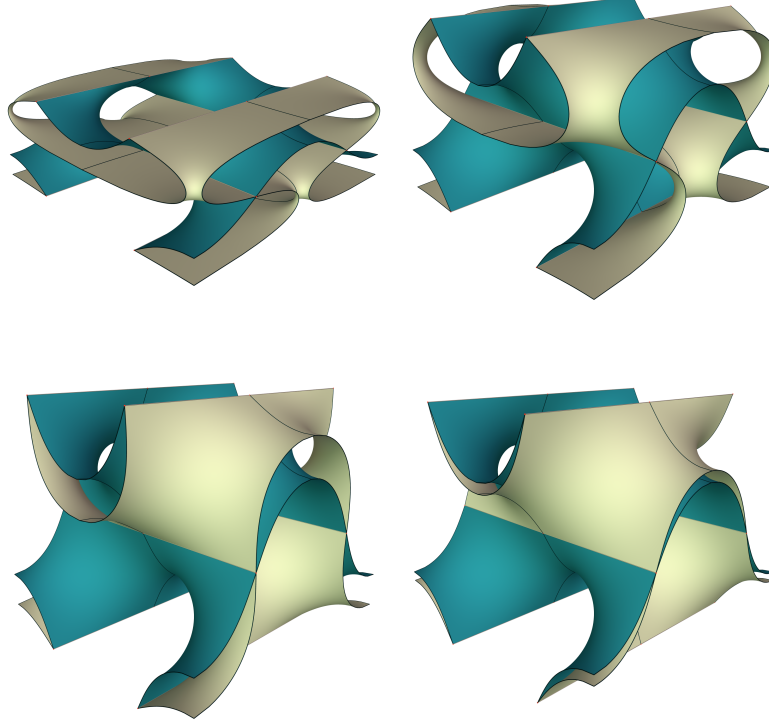


FIGURE 1.3. Comparison of oD (dark) and $\text{o}\Delta$ (bright) surfaces with the same lattice. These surfaces actually belong to the tD and $\text{t}\Delta$ subfamily.

The $\text{o}\Delta$ family is not merely a surprise. Its significance is revealed in the following proposition.

Proposition 1.3. *The surfaces in $\text{o}\Delta$ do not belong to the Meeks family. That is, the branched values of the Gauss map of an $\text{o}\Delta$ surface do not form four antipodal pairs. In fact, the only Meeks surfaces in \mathcal{D} are the oD surface. However, the closure $\overline{\text{o}\Delta}$ intersects oD in a 1-parameter family of TPMS.*

We now provide some context for the proposition.

For the purpose of this paper, a TPMS is a complete, embedded minimal surface $\tilde{\Sigma}$ in Euclidean space \mathbb{R}^3 invariant under a lattice Λ of Euclidean translations. The quotient $\Sigma = \tilde{\Sigma}/\Lambda$ then is a compact Riemann surface in the 3-torus \mathbb{R}^3/Λ . The lowest possible genus for a non-trivial TPMS is 3. In this case, the Gauss map of Σ has degree 2, and the surface is therefore necessarily hyperelliptic.

The first examples of TPMS were given by H. A. Schwarz [Sch90] around 1867, with explicit Weierstrass data for very symmetric cases. Schwarz understood that the eight branched values of the Gauss map play a crucial role. More generally, W. Meeks III [Mee90] explicitly constructed a family \mathcal{M} of TPMS of genus 3. He showed that if eight points on the sphere come in four antipodal pairs, then they are the branched values of the Gauss map for two conjugate TPMS of genus 3. The Meeks family \mathcal{M} , considered up to congruence and dilation, is a connected, smooth, (real) 5-dimensional manifold, and includes almost all previously known examples.

Famous exceptions are the H surfaces of Schwarz, for which the branched values are placed at the north pole, the south pole, and the vertices of a prism over an equilateral triangle inside the sphere; and the Gyroid of A. Schoen [Sch70], whose Gauss map has the same branched values as those of Schwarz' P and D surfaces, but does not belong to the Meeks family. We use \mathcal{N} to denote the complement of \mathcal{M} in the set of all TPMS of genus 3. Since then, more examples in \mathcal{N} have been found, either as isolated examples or as 1-parameter families, and some of them only numerically [FHL93, FH99, Wey06, Wey08]. Our 2-parameter family $\text{o}\Delta$ is therefore an important step towards the understanding of non-Meeks TPMS of genus 3.

Meeks' result is extended into the following rigidity statement: In the neighborhood of a non-degenerate TPMS, there is a bijection between TPMS and lattices in \mathbb{R}^3 ; see [KPS14] for instance. Hence up to congruence and dilation, a non-degenerate TPMS belongs (locally) to a 5-parameter family. Besides that, very little is known about the structure of \mathcal{N} . We would like to conjecture that \mathcal{N} is, like \mathcal{M} , connected and smooth, but none of these is known.

There is evidence [FHL93, FH99, Wey06, Wey08] that \mathcal{M} and the closure $\overline{\mathcal{N}}$ have non-empty intersection. Proposition 1.3 provides the first concrete example of such intersection in the form of a 1-dimensional family of TPMS. This is of considerable importance for stability questions of TPMS.

A TPMS of genus 3 is called a *bifurcation instance* if there are non-congruent deformations (bifurcation branches) of the TPMS with the same deformation of the lattice. Koiso, Piccione and Shoda [KPS14] identified isolated *bifurcation instances* among classical deformations of TPMS; see also [ES14, ES18]. They found bifurcation branches for most of these bifurcation instances. But for three “exotic” bifurcation instances, they only suggested that a bifurcation branch from them would not be a “classical” TPMS.

The intersection $\overline{\text{o}\Delta} \cap \text{oD}$ is a 1-parameter family of bifurcation instances. In particular, a 1-parameter subfamily of $\text{o}\Delta$, which we call $\text{t}\Delta$, has the same tetragonal lattices as the tD family. The intersection $\overline{\text{t}\Delta} \cap \text{tD}$ contains a single TPMS, denoted by tD^* , which turns out to be one of the exotic bifurcation instances in [KPS14].

We also find a bifurcation branch $t\Pi$ from the conjugate of tD^* , another exotic bifurcation instance in Schwarz' tP family. But $t\Pi$ is not the focus of this paper, since it is nothing but a classical oPa deformation [FK89, FH92].

For sufficiently large A and B , the existence of $o\Delta$ surfaces is implied by results of Traizet [Tra08], who constructed TPMS by opening catenoidal nodes among 2-tori. The positions of the nodes have to satisfy a balance condition, formulated in terms of elliptic functions, and a non-degeneracy condition. The Traizet limit of $o\Delta$ was noted by the first author in an earlier experimental work [Che18]. He used Brakke's Surface Evolver [Bra92] to numerically deform the TPMS from near the Traizet limit up to Schwarz' tD family, and obtained the first images of $t\Delta$. In particular, he observed that $t\Delta$ eventually intersects tD , but Surface Evolver fails to converge near the intersection. This failure can now be explained by numeric bifurcation.

Our paper is organized as follows:

In Section 2, we describe the Weierstrass data for surfaces in \mathcal{D} , prove their embeddedness, and formulate the period problem, depending on three real positive parameters a, b and t . The case $a = b$ corresponds to the oD surfaces, where the period problem is automatically solved. In the case $a \neq b$, the period problem becomes 1-dimensional but is rather complicated.

In Section 3 we show that, if $a \neq b$, the branched values of the Gauss map can *not* be antipodal. This proves that $\mathcal{D} \cap \mathcal{M} = oD$, and that any solution with $a \neq b$ (namely $o\Delta$) lies in \mathcal{N} .

Section 4 is dedicated to the existence proof of $o\Delta$. We show that for any choice of $a \neq b$, there is a value of t that solves the period problem. This is accomplished through a careful asymptotic analysis of the period integrals. We also conjecture the uniqueness of t based on numerical experiments.

To prove that $oD \subset \mathcal{M}$ and the closure of $o\Delta \subset \mathcal{N}$ have a non-empty intersection, we consider in Section 5 a modified period problem that eliminates the trivial solutions coming from oD . It turns out that this period problem can be solved explicitly in terms of elliptic integrals.

In section 6 we consider the surfaces with tetragonal lattices. They are \mathcal{D} surfaces whose parameters satisfy $ab = t$. In this case, we obtain two 1-parameter families of surfaces: $tD \subset oD$ containing Schwarz' D surface, and $t\Delta \subset o\Delta$. The intersection $t\Delta \cap tD$ contains a single TPMS tD^* . As the existence of $t\Delta$ does not follow from Section 4, we give an independent proof for this case using an extremal length argument.

Acknowledgements. The first author thanks his newborn daughter for keeping him awake through the nights, which helped noticing the $t\Delta$ family.

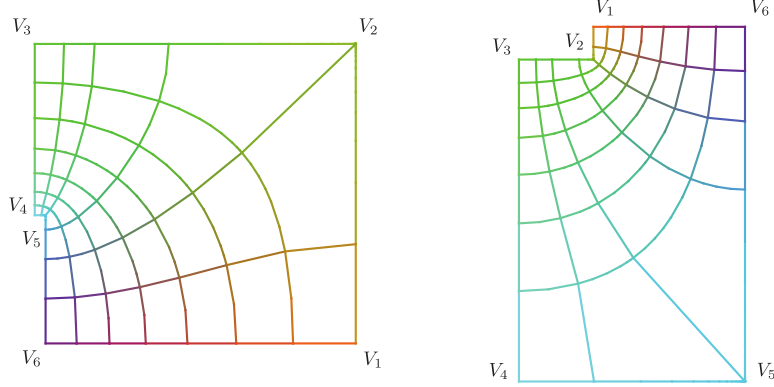
The second author thanks his teenage daughter for keeping him sleepless as well, thus providing time to work on this paper.

We are grateful to the anonymous referee for suggestions and corrections after carefully reading a previous version of the manuscript.

2. WEIERSTRASS DATA AND PERIOD PROBLEM

We parameterise a surface in \mathcal{D} with a Weierstrass representation defined on the upper half plane such that the real axis is mapped to the boundary of the hexagon S . Let the vertices of S be labeled by V_1, V_2, \dots, V_6 as in Figure 1.1 (left). Denote the preimage of V_k by $v_k \in \mathbb{R}$, and assume that $v_1 < v_2 < \dots < v_6$.

Given a \mathcal{D} surface, denote by dh its height differential and by G its Gauss map. Let $\phi_1 := dh \cdot G$ and $\phi_2 := dh/G$. The assumed boundary symmetries of the surface imply that $\Phi_j : z \mapsto \int^z \phi_j$ ($j = 1$ or 2) map the upper half plane to "right angled"

FIGURE 2.1. Images of a fundamental piece under Φ_1 and Φ_2 .

Euclidean hexagons. The interior angle is 270° at $\Phi_1(v_5)$ and $\Phi_2(v_2)$. Indeed, the Gauss map is vertical at V_2 and V_5 , hence v_2 and v_5 are respectively the pole and the zero of G . Interior angles at all other vertices are 90° ; see Figure 2.1.

Such maps are given by Schwarz-Christoffel maps. More specifically, we have

$$\begin{aligned}\phi_1 &:= \rho (z - v_1)^{-1/2} (z - v_2)^{-1/2} (z - v_3)^{-1/2} (z - v_4)^{-1/2} (z - v_5)^{+1/2} (z - v_6)^{-1/2} dz, \\ \phi_2 &:= -\frac{1}{\rho} (z - v_1)^{-1/2} (z - v_2)^{+1/2} (z - v_3)^{-1/2} (z - v_4)^{-1/2} (z - v_5)^{-1/2} (z - v_6)^{-1/2} dz, \\ dh &:= -i (z - v_1)^{-1/2} \times (z - v_3)^{-1/2} (z - v_4)^{-1/2} \times (z - v_6)^{-1/2} dz.\end{aligned}$$

Here, the real positive López-Ros factor ρ determines scaling of the image domains. The Gauss map is $G := i\rho(z - v_2)^{-1/2}(z - v_5)^{+1/2}$.

Proposition 2.1. *Up to congruence and dilation, the image of the upper half plane under the map*

$$(2.1) \quad z \mapsto \operatorname{Re} \int^z (\omega_1, \omega_2, \omega_3) = \operatorname{Re} \int^z \left(\frac{1}{2}(\phi_2 - \phi_1), \frac{i}{2}(\phi_2 + \phi_1), dh \right)$$

is almost the fundamental hexagon of a \mathcal{D} surface in the following sense: The intervals v_1v_2 , v_2v_3 , v_4v_5 and v_5v_6 are mapped to planar symmetry curves in the lateral faces of an axis parallel box. The intervals v_6v_1 and v_3v_4 are mapped, respectively, to straight segments parallel to the x and y axis, but not necessarily in the middle, in the bottom and top faces of the box.

Proof. Note that the integrand in ϕ_1 (resp. ϕ_2) is real positive (resp. negative) for $z > v_6$. This implies that the image of the segment v_6v_1 under the Schwarz-Christoffel map Φ_1 (resp. Φ_2) is horizontal rightward (resp. leftward), as in Figure 2.1.

The Schwarz-Christoffel maps Φ_j and $z \mapsto \int^z dh$ can be continued by reflection across any edge to the lower half plane, inducing symmetries of the minimal surface. We now determine what kind of symmetry is induced on each edge.

For that, we only carry out a detailed analysis on the edge v_6v_1 . The integrands in both ϕ_j are real on v_6v_1 , hence their continuations across this edge are given by $\overline{\phi_j(z)}$. Meanwhile, the integrand in dh is imaginary on v_6v_1 , so its continuation is given by $-\overline{dh(z)}$. Therefore, after crossing v_6v_1 , $\operatorname{Re} \omega_1$ remains unchanged while $\operatorname{Re} \omega_2$ and $\operatorname{Re} \omega_3$ change sign. This means that the surface is extended by a rotation about a straight line parallel to the x -axis.

Similar analysis on the other edges then prove that the image of the upper half plane under (2.1) has the claimed boundary curves. Note that the surface obtained

is free of singularities. Indeed, the metric is regular away from v_k , and the exponents at v_k guarantee a smooth extension. \square

We now study the condition for the two horizontal segments to lie in the middle of the top and the bottom faces of the box. To this end, we introduce notations for the edge lengths of the Euclidean hexagons

$$I_k := \left| \int_{v_k}^{v_{k+1}} \phi_1 \right|, \quad J_k := \left| \int_{v_k}^{v_{k+1}} \phi_2 \right|$$

for $1 \leq k \leq 5$. These are positive real numbers that depend analytically on the parameters v_1, \dots, v_6 and ρ .

Proposition 2.2. *The image of the upper half plane under the Weierstrass representation (2.1) is the fundamental hexagon of a surface in \mathcal{D} if and only if the following period conditions are satisfied:*

$$(2.2) \quad \begin{aligned} I_1 + I_5 &= J_1 + J_5 \\ I_2 + I_4 &= J_2 + J_4 \end{aligned}$$

Proof. The bottom segment V_6V_1 lies in the middle of the bottom face if and only if

$$\operatorname{Re} \int_{v_1}^{v_2} \omega_2 = \operatorname{Re} \int_{v_5}^{v_6} \omega_2.$$

This is equivalent to

$$\operatorname{Im} \int_{v_1}^{v_2} (\phi_2 + \phi_1) = \operatorname{Im} \int_{v_5}^{v_6} (\phi_2 + \phi_1).$$

Observe on v_1v_2 that the integrand in ϕ_1 (resp. ϕ_2) is positive (resp. negative) imaginary, and on v_5v_6 that the integrand in ϕ_1 (resp. ϕ_2) is negative (resp. positive) imaginary. So the equation above can be written as

$$I_1 - J_1 = J_5 - I_5,$$

which proves the first period condition. The second follows analogously. \square

We can eliminate ρ by taking the quotient of the two equations, therefore:

Corollary 2.3. *If*

$$Q_I := \frac{I_1 + I_5}{I_2 + I_4} = \frac{J_1 + J_5}{J_2 + J_4} =: Q_J$$

or, equivalently, if

$$(2.3) \quad Q := Q_I - Q_J = \frac{I_1 + I_5}{I_2 + I_4} - \frac{J_1 + J_5}{J_2 + J_4} = 0$$

for some choice of v_1, \dots, v_6 , then $\rho \in \mathbb{R}_{>0}$ can be uniquely adjusted so that the period conditions (2.2) are satisfied.

Thus we have expressed the period condition as a single equation $Q = 0$, where Q depends on six parameters v_1, \dots, v_6 . The number of parameters can be reduced to three after a normalization by Möbius transformations. More specifically, we can assume

$$v_1 = -t, v_2 = -a, v_3 = -1, v_4 = 1, v_5 = b, v_6 = t$$

with $-t < -a < -1 < 1 < b < t$. We also assume that $a \leq b$. If it is not the case, we may simply switch a and b ; this only exchanges I_k and J_{6-k} , $1 \leq k \leq 5$, up to the scaling ρ , hence leaves Q invariant.

We note two special cases.

If $a = b$, the period conditions (2.2) are satisfied automatically with $\rho = 1$. In this case, the involution $z \mapsto -\bar{z}$ induces an order-2 rotation of the surface about a

vertical axis. This can be seen by noting that ω_1 and ω_2 change sign but ω_3 keeps sign under this involution. Indeed, on the imaginary axis (fixed by the involution), ϕ_1 and ϕ_2 are conjugate and dh is real. Hence the positive imaginary axis is mapped by the Weierstrass representation (2.1) to the vertical straight segment between the middle points of V_3V_4 and of V_6V_1 , which serves as the axis of the order-2 rotation. This shows that the surface is in oD.

If $ab = t$, we will see in Section 6 that the period conditions are satisfied with $Q_I = Q_J = 1$ and $\rho^4 = a/b$. In this case, the involution $\iota : z \mapsto -t/z$ induces an order-2 orientation-preserving rotation of the surface around a horizontal axis, because

$$\iota^*dh = -dh \quad \text{and} \quad G(\iota(z))G(z) = i.$$

This rotation exchanges V_k with V_{k+3} , $1 \leq k \leq 3$. In particular, the segments V_6V_1 and V_3V_4 must have the same length, implying that the bounding box has a square base. The unique fixed point of the involution, namely $i\sqrt{t}$, is mapped to the fixed point of the rotation. We will consider this case in detail in Section 6.

Proposition 2.4. *The minimal hexagons S in \mathcal{D} are embedded. Consequently, the triply periodic minimal surfaces generated by extending across symmetry lines are embedded as well.*

Proof. Denote the projection onto the xz -plane by ϖ , and let $V'_i = \varpi(V_i)$. We will prove (referring to Figure 1.1 (left)):

- (1) The boundary of S is a graph over a simple curve γ in the xz -plane, except for the straight segment V_3V_4 which is parallel to the y -axis. Thus γ bounds a simply connected (open) domain Ω .

To see this, note that the Gauss map $G := i\rho(z - v_2)^{-1/2}(z - v_5)^{1/2}$ is horizontal (i.e. perpendicular to the y -direction) along the segments $V_2V_3V_4V_5$ and strictly monotone. This implies that the arcs $V'_2V'_3$ and $V'_4V'_5$ of γ are simple, disjoint, and lie in the rectangle $[-A, A] \times [0, 1]$. The remaining segments $V'_5V'_6$, $V'_6V'_1$ and $V'_1V'_2$ are straight segments on the boundary of that rectangle.

- (2) The projection $\varpi(S)$ lies within $\overline{\Omega}$.

To see this, assume the opposite. Take a boundary point of $\varpi(S)$ that does not lie in $\overline{\Omega}$. By (the contraposition of) the Implicit Function Theorem, its preimage on the S has a horizontal normal (parallel to the xz -plane). By the formula for the Gauss map, the only points with horizontal normal occur on the boundary of S , a contradiction.

- (3) The projection ϖ restricted to the interior of S has the unique path and homotopy lifting properties.

To see this, we again use that the interior of S has no point with horizontal normal. The claim follows from the Implicit Function Theorem, applied in the compact region where the curve (or homotopy) resides.

Then it follows that the interior of S is a graph over Ω : Otherwise, take a curve on S that connects two distinct points in $\varpi^{-1}(p)$, $p \in \Omega$. Its projection onto Ω is closed in Ω and can be retracted onto p within a compact subset of Ω . By the unique homotopy lifting property, the endpoints of the lifted curves stay the same, contradicting the assumption that they are two distinct points in $\varpi^{-1}(p)$. \square

3. BRANCHED VALUES OF THE GAUSS MAP

To locate the branched points of the Gauss map, we use the following simple observation:

Lemma 3.1. *At every orthogonal intersection of a planar symmetry curve and a straight line on a minimal surface, the Gauss map has a branched point.*

Proof. At points on the straight line that are symmetric with respect to the symmetry plane, the Gauss map takes the same value. Hence it cannot be single valued in a neighborhood of the intersection point. \square

We now show

Theorem 3.2. *The branched values of the Gauss map of a surface in \mathcal{D} are antipodal if and only if $a = b$.*

Proof. By the Lemma, the Gauss map has branched points at V_1, V_3, V_4 and V_6 . On a translational fundamental domain, each of these points occurs twice, giving eight branched points as expected.

Recall that the stereographically projected Gauss map is given by

$$G(z) = i\rho(z + a)^{-1/2}(z - b)^{+1/2}.$$

We then compute the branched values explicitly as

$$\begin{aligned} \pm G(+1) &= \mp \rho \sqrt{\frac{b-1}{a+1}}, & \pm G(-1) &= \mp \rho \sqrt{\frac{b+1}{a-1}}, \\ \pm G(+t) &= \pm i \rho \sqrt{\frac{t-b}{t+a}}, & \pm G(-t) &= \pm i \rho \sqrt{\frac{t+b}{t-a}}. \end{aligned}$$

Recall that $-t < -a < -1 < 1 < b < t$, so the expressions under the square roots are all positive real. We then see that they lie on the real and imaginary axis, respectively, which helps matching them in possible antipodal pairs. Recall that, after stereographic projection, the antipodal point of z is $-1/\bar{z}$.

Assume that the branched values do occur in antipodal pairs and, for the sake of contradiction, that $a \neq b$. First note that $G(+1)$ and $-G(+1)$ cannot be antipodal. Otherwise, $G(-1)$ and $-G(-1)$ must also be antipodal. Then they must have the same norm, i.e. $\frac{b-1}{a+1} = \frac{b+1}{a-1}$, forcing $a + b = 0$ which violates our assumption. Thus the only possibility is that $\pm G(-1)$ and $\pm G(+1)$ are antipodal, with two possible choices of signs. Either choice implies that

$$\rho^4 = \frac{a^2 - 1}{b^2 - 1}.$$

The same analysis on $\pm G(\pm t)$ leads to

$$\rho^4 = \frac{t^2 - a^2}{t^2 - b^2}.$$

Combining the two equations for ρ^4 shows, after a brief computation, that either $t = 1$ or $a = b$. The contradiction with our assumptions proves the “only if”.

For the “if” part, assume that $a = b$. Then we find the branched points become antipodal (only) with $\rho = 1$. More specifically, we have

$$\begin{aligned} \pm G(+1) &= \mp \sqrt{\frac{a-1}{a+1}}, & \pm G(-1) &= \mp \sqrt{\frac{a+1}{a-1}}, \\ \pm G(+t) &= \pm i \sqrt{\frac{t-a}{t+a}}, & \pm G(-t) &= \pm i \sqrt{\frac{t+a}{t-a}}. \end{aligned}$$

Geometrically, these points on the unit sphere are vertices of two axis parallel rectangles in the planes $x = 0$ and $y = 0$, respectively. Remarkably, an image of two such rectangles already appears in Figure 44 of the *Nachtrag* of Schwarz’ paper “Bestimmung einer speziellen Minimalfläche” from 1867. \square

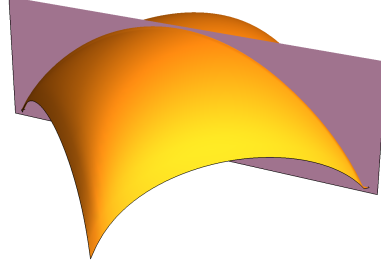


FIGURE 4.1. Numerical plot of the solution set of $Q(a, b; t) = 0$. The vertical plane in gray is the set of trivial solutions with $a = b$ corresponding to the oD surfaces. The other surface is the set of non-trivial solutions corresponding to the o Δ surfaces.

We note that in the case $a = b$ the branched values lie at the vertices of a cube if and only of $a^2 = b^2 = t = 3$. This is the case of the classical D surface of Schwarz.

4. EXISTENCE OF NON-TRIVIAL SOLUTIONS

Recall that $1 < a \leq b < t$, and the periodic condition (2.3) as we copy below

$$Q(a, b; t) = \frac{I_1 + I_5}{I_2 + I_4} - \frac{J_1 + J_5}{J_2 + J_4} = 0.$$

The quantity Q is our focus in the remaining of this paper. From now on, we will ignore the Lopéz-Ros factor ρ in our calculations, since Q is independent of this factor.

We now prove the main theorem of this paper.

Theorem 4.1. *If $a = b$, the period condition (2.3) is solved for any choice of t . If $a < b$, then there exists a value of t that solves the period condition (2.3).*

The solution set of $Q(a, b; t) = 0$ is numerically plotted in Figure 4.1. The case $a = b$, shown here as a vertical plane in gray, has been discussed in Section 2. The case $a < b$, as well as our main theorem, follows from the continuity of Q in t , and the following proposition.

Proposition 4.2. *If $1 < a < b < t$ then*

$$(4.1) \quad \lim_{t \rightarrow b+} Q(a, b; t) > 0,$$

$$(4.2) \quad \lim_{t \rightarrow +\infty} Q(a, b; t) = -\infty.$$

The remainder of this section is devoted to the proof of this proposition.

We begin by analyzing the limit $t \rightarrow b+$.

Proof of (4.1). We can evaluate the period integrals explicitly. Recall that, if $p < q$, we have

$$\int_p^q \sqrt{\frac{1}{(q-z)(z-p)}} dz = \pi, \quad \int_p^q \sqrt{\frac{z-p}{q-z}} dz = \frac{q-p}{2} \pi.$$

By the Mean Value Theorem for integrals, we have

$$\lim_{t \rightarrow b+} I_1(a, b; t) = \lim_{t \rightarrow b+} \int_{-t}^{-a} \frac{1}{\sqrt{(t^2 - z^2)(z^2 - 1)}} \sqrt{\frac{b-z}{-a-z}} dz = C \int_a^b \sqrt{\frac{1}{(b-z)(z-a)}} dz,$$

where $C = 1/\sqrt{c^2 - 1}$ for some $c \in [a, t]$. So this limit is finite and non-zero. Similarly,

$$\begin{aligned} \lim_{t \rightarrow b+} I_2(a, b; t) &= C \int_1^a \sqrt{\frac{1}{(a-z)(z-1)}} dz, \\ \lim_{t \rightarrow b+} J_1(a, b; t) &= C \int_a^b \sqrt{\frac{z-a}{b-z}} dz, \quad \lim_{t \rightarrow b+} J_2(a, b; t) = C \int_1^a \sqrt{\frac{z-1}{a-z}} dz, \\ \lim_{t \rightarrow b+} I_4(a, b; t) &= C \int_1^b \sqrt{\frac{1}{z-1}} dz, \quad \lim_{t \rightarrow b+} J_5(a, b; t) = C \lim_{t \rightarrow b+} \int_b^t \sqrt{\frac{1}{(t-z)(z-b)}} dz \end{aligned}$$

are all finite and non-zero. Here C denote any finite positive number. On the other hand,

$$\lim_{t \rightarrow b+} I_5(a, b; t) = C \lim_{t \rightarrow b+} \int_b^t \sqrt{\frac{z-b}{t-z}} dz = 0$$

and

$$\lim_{t \rightarrow b+} J_4(a, b; t) \geq C \lim_{t \rightarrow b+} \int_1^b \sqrt{\frac{1}{(t-z)(b-z)}} dz$$

diverges to infinity. Consequently, as $t \rightarrow b+$, $Q_I = (I_1 + I_5)/(I_2 + I_4)$ has a finite and non-zero limit, while $Q_J = (J_1 + J_5)/(J_2 + J_4) \rightarrow 0$, hence $\lim_{t \rightarrow b+} Q > 0$. \square

Now we turn to the limit $t \rightarrow \infty$, which is more amusing.

Proof of (4.2). For the periods in the denominators, we note that

$$\begin{aligned} \lim_{t \rightarrow \infty} t \cdot I_2(a, b; t) &= \int_{-a}^{-1} \sqrt{\frac{1}{z^2 - 1}} \sqrt{\frac{b-z}{a+z}} dz, \\ \lim_{t \rightarrow \infty} t \cdot J_2(a, b; t) &= \int_{-a}^{-1} \sqrt{\frac{1}{z^2 - 1}} \sqrt{\frac{a+z}{b-z}} dz, \\ \lim_{t \rightarrow \infty} t \cdot I_4(a, b; t) &= \int_1^b \sqrt{\frac{1}{z^2 - 1}} \sqrt{\frac{b-z}{a+z}} dz, \\ \lim_{t \rightarrow \infty} t \cdot J_4(a, b; t) &= \int_1^b \sqrt{\frac{1}{z^2 - 1}} \sqrt{\frac{a+z}{b-z}} dz \end{aligned}$$

are all finite. We now show that

$$(4.3) \quad \lim_{t \rightarrow \infty} t \cdot (I_2 + I_4) > \lim_{t \rightarrow \infty} t \cdot (J_2 + J_4),$$

or equivalently,

$$\lim_{t \rightarrow \infty} t \cdot (I_2 - J_2) > \lim_{t \rightarrow \infty} t \cdot (J_4 - I_4).$$

We prove this by considering the functions

$$\begin{aligned} f(a, b) &= \lim_{t \rightarrow \infty} t \cdot (I_2 - J_2) = \int_1^a \frac{2z - a + b}{\sqrt{(z^2 - 1)(a - z)(b + z)}} dz, \\ g(a, b) &= \lim_{t \rightarrow \infty} t \cdot (J_4 - I_4) = \int_1^b \frac{2z + a - b}{\sqrt{(z^2 - 1)(a + z)(b - z)}} dz, \end{aligned}$$

and show that $f(a, b) > g(a, b)$ for all $1 < a < b$. Note that $f(a, b) = g(b, a)$. Since

$$\frac{\partial}{\partial b} f(a, b) = \int_1^a \frac{a + b}{\sqrt{(z^2 - 1)(a - z)(b + z)^3}} dz > 0,$$

f is monotone increasing in its second argument for $1 < a < b$. Then g is monotone increasing in its first argument. Note also that $f(a, a) = \pi$ is a constant. Hence

$$f(a, b) > f(a, a) = f(b, b) = g(b, b) > g(a, b),$$

which finishes the proof of (4.3).

The periods in the numerators are more delicate to deal with, as they have logarithmic asymptotics. For instance,

$$\begin{aligned}
 t \cdot J_5(a, b; t) &= \int_b^t \frac{t}{\sqrt{t^2 - z^2}} \sqrt{\frac{z+a}{z-b}} \sqrt{\frac{1}{z^2 - 1}} dz \\
 &> \int_b^t \frac{t}{\sqrt{t^2 - z^2}} \frac{1}{z} dz \\
 &= \log \frac{\sqrt{t^2 - b^2} + t}{b},
 \end{aligned}
 \tag{4.4}$$

hence $t \cdot J_5(a, b; t)$ diverges to $+\infty$ as $t \rightarrow \infty$.

Fortunately, the integrals I_1 and J_1 (and I_5 and J_5) have the same logarithmic singularities. By the dominated convergence theorem, we obtain the following estimates:

$$\begin{aligned}
 \lim_{t \rightarrow \infty} t \cdot (I_1 - J_1) &= \lim_{t \rightarrow \infty} \int_{-t}^{-a} \frac{t(a+b)}{\sqrt{(t^2 - z^2)(z^2 - 1)(b-z)(-a-z)}} dz \\
 &= \int_{-\infty}^{-a} \frac{a+b}{\sqrt{z^2 - 1} \sqrt{b-z} \sqrt{-a-z}} dz, \\
 \lim_{t \rightarrow \infty} t \cdot (I_5 - J_5) &= \lim_{t \rightarrow \infty} \int_b^t \frac{-t(a+b)}{\sqrt{t^2 - z^2} \sqrt{z^2 - 1} \sqrt{z-b} \sqrt{z+a}} dz \\
 &= \int_b^{\infty} \frac{-a-b}{\sqrt{z^2 - 1} \sqrt{z-b} \sqrt{z+a}} dz.
 \end{aligned}
 \tag{4.5}$$

Note that they are finite and non-zero.

Finally, we write

$$Q(a, b; t) = \frac{t(I_1 - J_1) + t(I_5 - J_5)}{tI_2 + tI_4} + t(J_1 + J_5) \left[\frac{1}{tI_2 + tI_4} - \frac{1}{tJ_2 + tJ_4} \right].$$

The part in the square bracket is negative by (4.3). As $t \rightarrow \infty$, the first fraction is bounded by (4.5), and $J_5 \rightarrow +\infty$. This then concludes the proof of the proposition. \square

Before ending this section, we propose the following uniqueness conjecture based on numeric experiments:

Conjecture 4.3. *If $a < b$, then there exists a unique t that solves the period condition (2.3).*

5. INTERSECTION WITH THE MEEKS-LOCUS

By definition, the two families $\text{oD} \subset \mathcal{M}$ and $\text{o}\Delta \subset \mathcal{N}$ are disjoint in \mathcal{D} . However, we will show in this section that the closure $\overline{\text{o}\Delta}$ intersects oD , and give an explicit description of the intersection in terms of elliptic integrals. This result is not strictly needed for this paper, but gives insight into the nature of the bifurcation locus.

To make this precise, we use on \mathcal{D} the topology induced by the space of possible Weierstrass data, which are determined by the four real parameters a, b, t and ρ . Clearly, the convergence of Weierstrass data implies the locally uniform convergence of the minimal surfaces.

The goal is to determine the intersection of the Meeks locus

$$\text{oD} = \{(a, b, t) : Q(a, b; t) = 0, a = b, -t < -a < -1 < 1 < b < t\}$$

with the closure of the non-Meeks locus

$$\text{o}\Delta = \{(a, b, t) : Q(a, b; t) = 0, a \neq b, -t < -a < -1 < 1 < b < t\}.$$

The idea is to divide the function $Q(a, b; t)$ by $b - a$ and take the limit for $a \rightarrow b$ to eliminate solutions in the Meeks locus. We claim:

Theorem 5.1. *The intersection $\overline{\text{oD}} \cap \text{oD}$ is described by the equation*

$$(5.1) \quad \bar{K}(m_1)E(m_2) + \bar{E}(m_1)K(m_2) = \bar{K}(m_1)K(m_2),$$

where

$$K(m) = \int_0^{\pi/2} \frac{1}{\sqrt{1 - m \sin^2(\theta)}} d\theta,$$

$$E(m) = \int_0^{\pi/2} \sqrt{1 - m \sin^2(\theta)} d\theta$$

are complete elliptic integrals of the first and the second kind, $\bar{K}(m) = K(1 - m)$ and $\bar{E}(m) = E(1 - m)$ are the associated elliptic integrals, and the moduli

$$m_1 = \frac{a^2 - 1}{t^2 - 1}, \quad m_2 = \frac{t^2 a^2 - 1}{a^2 t^2 - 1}.$$

Note that $0 < m_1 < m_2 < 1$.

Remark 5.2. It is interesting to notice the similarity of (5.1) with the Legendre relation $\bar{K}(m)E(m) + \bar{E}(m)K(m) - \bar{K}(m)K(m) = \pi/2$.

Before we sketch the technical proof, we note that the function Q can be extended to a holomorphic function of its arguments a, b and t for a near b . To see this, note that the integrand of each of the integrals I_k and J_k used in the definition of Q can be adjusted by multiplication with a constant factor e^{it} so that the absolute values are not necessary. The square roots of the integrands cause a potential multivaluedness when the roots $-t, -a, b$ and t are close to each other, which is not the case for a near b . As $Q(a, a, t) = 0$, this implies that also \tilde{Q} extends to a holomorphic function of its arguments. In particular, the extension of \tilde{Q} for real arguments is real analytic.

The theorem follows from the following proposition:

Proposition 5.3. *The function*

$$\tilde{Q}(a, b; t) = \frac{1}{b - a} Q(a, b; t)$$

extends analytically to $a = b$ by

$$\tilde{Q}(a, a; t) = \frac{a(t^2 - 1)}{(a^2 - 1)(t^2 - a^2)} \frac{\bar{K}(m_1)K(m_2) - \bar{K}(m_1)E(m_2) - \bar{E}(m_1)K(m_2)}{K(m_2)^2}.$$

Remark 5.4. Technical details in the following proof are omitted. The integrals we need can all be evaluated in terms of the complete elliptic integrals of the first and the second kind. Integral tables in [BF71] have been very helpful for this purpose, especially after a well-known computer algebra system failed us here.

Proof. With the help of the integral tables in [BF71], we obtain the following explicit evaluation of the periods.

$$(I_1 + I_5)(a, a; t) = (J_1 + J_5)(a, a; t) = \frac{2\bar{K}(m_1)}{\sqrt{t^2 - 1}},$$

$$(I_2 + I_4)(a, a; t) = (J_2 + J_4)(a, a; t) = \frac{2K(m_2)}{\sqrt{t^2 - 1}}.$$

Then we evaluate the derivatives

$$I'_k(a, a; t) = \frac{\partial}{\partial b} \Big|_{a=b} I_k(a, b, t), \quad J'_k(a, a; t) = \frac{\partial}{\partial b} \Big|_{a=b} J_k(a, b, t),$$

and obtain

$$\begin{aligned} (I'_2 + I'_4)(a, a; t) &= \frac{K(m_2)}{a\sqrt{t^2-1}}, & (I'_1 + I'_5)(a, a; t) &= 0, \\ (J'_1 + J'_5)(a, a; t) &= \frac{2a\bar{K}(m_1)}{\sqrt{t^2-1}(t^2-a^2)} - \frac{2a\bar{E}(m_1)\sqrt{t^2-1}}{(a^2-1)(t^2-a^2)}, \\ (J'_2 + J'_4)(a, a; t) &= \frac{K(m_2)}{a\sqrt{t^2-1}} - \frac{2aK(m_2)}{\sqrt{t^2-1}(a^2-1)} + \frac{2aE(m_2)\sqrt{t^2-1}}{(a^2-1)(t^2-a^2)}. \end{aligned}$$

Finally, by L'Hôpital,

$$\begin{aligned} (5.2) \quad \lim_{a \rightarrow b} \frac{1}{b-a} Q(a, b; t) &= \frac{\partial Q}{\partial b} \Big|_{a=b} \\ &= \frac{a(t^2-1)}{(a^2-1)(t^2-a^2)} \frac{\bar{K}(m_1)K(m_2) - \bar{K}(m_1)E(m_2) - \bar{E}(m_1)K(m_2)}{K(m_2)^2}. \end{aligned}$$

□

6. THE TETRAGONAL CASE

We denote by \mathcal{T} surfaces in \mathcal{D} with tetragonal lattice. That is, their unit cells are prisms over squares. We have seen that this occurs when $ab = t$. Again, we have the classical family $t\mathcal{D} = o\mathcal{D} \cap \mathcal{T}$ when $a = b = \sqrt{t}$. The final specialization arises when $t = 3$. In this case, all diagonals and midpoint bisectors of the embedded minimal hexagon are straight lines, and we have the classical D surface.

In this section we will show that $t\Delta = o\Delta \cap \mathcal{T}$ is non-empty and, in fact, contains a 1-parameter family of surfaces meeting $t\mathcal{D}$ on its boundary. More specifically, these surfaces are characterized by $ab = t$, hence they all admit a conformal involution, that exchanges V_k with V_{k+3} , $1 \leq k \leq 3$.

Lemma 6.1. *When $ab = t$, the period condition is solved if and only if $I_1 + I_5 = I_2 + I_4$, in which case $\rho^4 = a/b$.*

Proof. The assumption $t = ab$ implies that

$$I_k = \rho^2 \sqrt{\frac{b}{a}} J_{k+3}, \quad \text{and} \quad J_k = \frac{1}{\rho^2} \sqrt{\frac{a}{b}} I_{k+3}$$

for $k = 1, 2, 3$. Therefore

$$Q_I = \frac{I_1 + I_5}{I_2 + I_4} = \frac{J_2 + J_4}{J_1 + J_5} = Q_J^{-1}.$$

Hence $Q = Q_I - Q_J = 0$ implies that $Q_I = 1$. □

We use this lemma to construct right angled hexagons that solve the period problem.

Begin with an axis parallel rectangle R of size $1 \times A$, where $1 < A < 2$ is the height; see Figure 6.1. Draw a line from the top left vertex of R in the 45° south-east direction. Choose a point p on this line in the lower half of R (possible because $A < 2$), and use it as the bottom right vertex of a smaller rectangle R' with the same symmetries. Cut the rectangular annulus between R and R' into four along the symmetry lines. The top right component is a right angled hexagon that solves the period problem.

Its conformal type, however, is still too general. It needs to have a holomorphic involution permuting the edges.

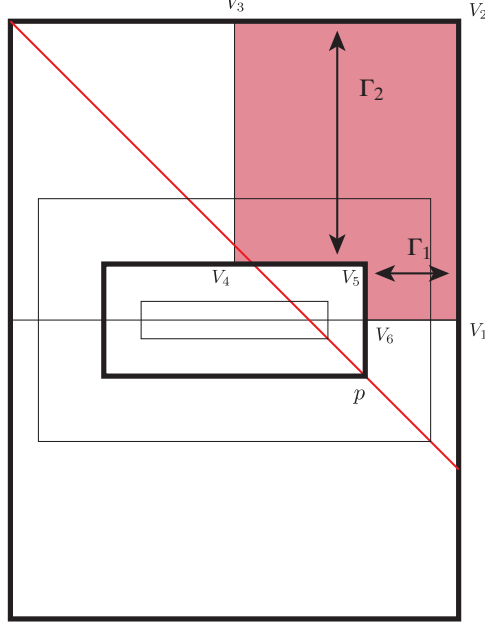


FIGURE 6.1. Existence Proof for $t\Delta$

Theorem 6.2. *For any choice of $1 < A < 2$, there is a choice of p so that the hexagon has a conformal involution.*

Proof. The proof uses an extremal length argument.

Consider the curve families Γ_1 and Γ_2 connecting edges as in Figure 6.1. These families are obtained from each other by the topological order 2 rotation. So in a conformally correct hexagon, they need to have the same extremal length.

Vice versa, we claim that if $\text{ext}\Gamma_1 = \text{ext}\Gamma_2$ then the hexagon has a conformal involution. To see this, we map the hexagon to the upper half plane by the inverse of the Schwarz-Christoffel map $z \mapsto \int^z \phi_1$. The hexagon vertices V_i are mapped to real numbers v_i , and the curve family Γ_1 is mapped to the curves family connecting the edge v_1v_2 with the edge v_5v_6 . Therefore its extremal length is that of the conformal rectangle $v_1v_2v_5v_6$, and thus determines the cross ratio of these four points. Similarly, the extremal length of Γ_2 determines the cross ratio of the four points $v_2v_3v_4v_5$. If we normalize the v_i as before, the equality of these cross ratios

$$\frac{(a+t)(b+t)}{2t(a+b)} = \frac{(a+1)(b+1)}{2(a+b)}$$

implies that $ab = t$, so the hexagon has indeed a conformal involution.

Thus we have to show that we can adjust the position of p so that the two extremal lengths are equal. Note that moving p to the left will pinch the vertical edge V_5V_6 , while moving p to the right will pinch the horizontal edge V_6V_1 . This shows that the extremal length of Γ_1 will vary between infinity and 0. On the other hand, during this variation, the extremal length of Γ_2 stays bounded away from 0 and infinity. Hence there must be a p for which $\text{ext}\Gamma_1 = \text{ext}\Gamma_2$. \square

Note that the $t\Delta$ family corresponds to the case when both rectangles degenerate to squares.

Remark 6.3. In the tetratonal case $ab = t$, the substitution $\zeta = z - t/z$ allows us to express the I_k 's in terms of the complete elliptic integral $K(\mu)$ with complex modulus

$$\mu = \frac{(1+a)(1-b)}{2} \frac{(\sqrt{t}-i)^2}{(t-1)} \frac{1}{(\sqrt{a}+i\sqrt{b})^2}.$$

Then the period condition in Lemma 6.1 is equivalent to

$$\cot \left(\arg \frac{K(\mu) + iK'(\mu)}{\sqrt{b} - i\sqrt{a}} \right) = \frac{\sqrt{b} - \sqrt{a}}{\sqrt{b} + \sqrt{a}}.$$

The intersection with tD can be determined explicitly using the equation from Section 5. Note that for $a = b = \sqrt{t}$, we have

$$m = m_2 = 1 - m_1 = \frac{a^2}{1 + a^2}.$$

Simplifying (5.1) shows that the intersection occurs when

$$2E(m) = K(m).$$

This is solved numerically with $a = a^* \approx 2.17966$. We use tD^* to denote the surface with parameters $a = b = \sqrt{t} = a^*$. In Figure 6.2 we compare Schwarz' D surface, the most symmetric surface in the tD family, with the surface tD^* at the junction of tD and $\text{t}\Delta$.

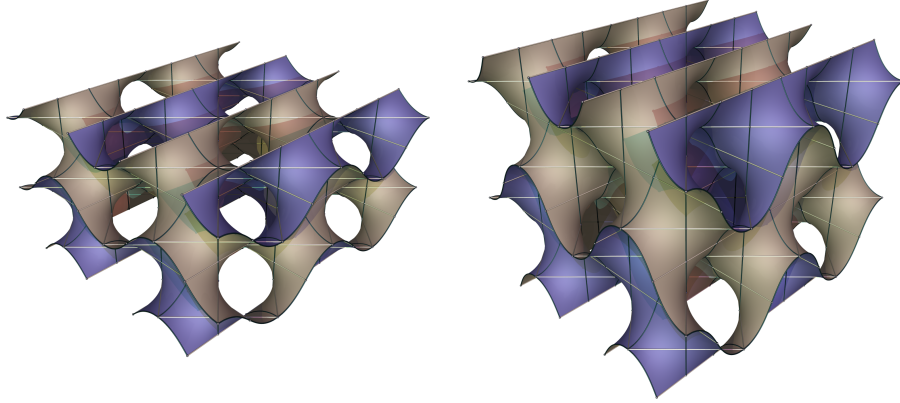


FIGURE 6.2. Schwarz' D and the unstable tD^* surface

The Gauss map of the tD^* surface has eight branched values at $\pm\alpha^{\pm 1}$ and $\pm\alpha^{\pm 1}i$, where $\alpha = \sqrt{(a^* - 1)/(a^* + 1)}$. They are the eight roots of $z^8 + kz^4 + 1 = 0$, where

$$k = \alpha^{-4} + \alpha^4 = \frac{(a^* - 1)^2}{(a^* + 1)^2} + \frac{(a^* + 1)^2}{(a^* - 1)^2} \approx 7.40284$$

This is precisely the value calculated by Koiso, Piccione and Shoda [KPS14] for a bifurcation instance in the tD family. An explicit bifurcation branch from tD^* was then missing, but now provided by the $\text{t}\Delta$ family.

Remark 6.4. Surprisingly, numerical computations show that, near the bifurcation point, $\text{t}\Delta$ surfaces have actually *smaller* area than the corresponding tD surfaces with the same lattice.

The conjugate of tD^* , denoted by tP^* , was identified in [KPS14] as a bifurcation instance in the tP family. We also find a bifurcation branch from tP^* , denoted by tII . As one deforms the tetragonal lattice, the horizontal handles deform uniformly along the tP branch. But along the tII branch, the handles in the x direction shrink while the handles in the y direction expand. The tII family turns out to be a subfamily of oPa , a 2-parameter orthorhombic deformation family of Schwarz P surface. Since $oPa \subset \mathcal{M}$, tII is less interesting for understanding non-Meeks surfaces, hence not a focus of the current paper.

REFERENCES

- [BF71] Paul F. Byrd and Morris D. Friedman. *Handbook of elliptic integrals for engineers and scientists*. Die Grundlehren der mathematischen Wissenschaften, Band 67. Springer-Verlag, New York-Heidelberg, 1971. Second edition, revised.
- [Bra92] Kenneth A. Brakke. The surface evolver. *Experiment. Math.*, 1(2):141–165, 1992.
- [Che18] Hao Chen. Minimal twin surfaces. *Exp. Math.*, 2018. online first.
- [ES14] Norio Ejiri and Toshihiro Shoda. On a moduli theory of minimal surfaces. In *Prospects of differential geometry and its related fields*, pages 155–172. World Sci. Publ., Hackensack, NJ, 2014.
- [ES18] Norio Ejiri and Toshihiro Shoda. The Morse index of a triply periodic minimal surface. *Differential Geom. Appl.*, 58:177–201, 2018.
- [FH92] Andrew Fogden and Stephen T. Hyde. Parametrization of triply periodic minimal surfaces. II. regular class solutions. *Acta Cryst. Sect. A*, 48(4):575–591, 1992.
- [FH99] Andrew Fogden and Stephan T. Hyde. Continuous transformations of cubic minimal surfaces. *The European Physical Journal B-Condensed Matter and Complex Systems*, 7(1):91–104, 1999.
- [FHL93] Andrew Fogden, M. Haeberlein, and Sven Lidin. Generalizations of the gyroid surface. *J. Phys. I*, 3(12):2371–2385, 1993.
- [FK89] Werner Fischer and Elke Koch. Genera of minimal balance surfaces. *Acta Cryst. Sect. A*, 45(10):726–732, 1989.
- [KPS14] Miyuki Koiso, Paolo Piccione, and Toshihiro Shoda. On bifurcation and local rigidity of triply periodic minimal surfaces in \mathbb{R}^3 , 2014. preprint, [arXiv:1408.0953](#).
- [LHM01] Hippolyte Lazard-Holly and William H. Meeks, III. Classification of doubly-periodic minimal surfaces of genus zero. *Invent. Math.*, 143(1):1–27, 2001.
- [Mee90] William H. Meeks, III. The theory of triply periodic minimal surfaces. *Indiana Univ. Math. J.*, 39(3):877–936, 1990.
- [MPR98] William H. Meeks, III, Joaquín Pérez, and Antonio Ros. Uniqueness of the Riemann minimal examples. *Invent. Math.*, 133(1):107–132, 1998.
- [MR05] William H. Meeks, III and Harold Rosenberg. The uniqueness of the helicoid. *Ann. of Math. (2)*, 161(2):727–758, 2005.
- [PRT05] Joaquín Pérez, M. Magdalena Rodríguez, and Martin Traizet. The classification of doubly periodic minimal tori with parallel ends. *J. Differential Geom.*, 69(3):523–577, 2005.
- [PT07] Joaquín Pérez and Martin Traizet. The classification of singly periodic minimal surfaces with genus zero and Scherk-type ends. *Trans. Amer. Math. Soc.*, 359(3):965–990, 2007.
- [Sch90] Hermann A. Schwarz. *Gesammelte Mathematische Abhandlungen*, volume 1. Springer, Berlin, 1890.
- [Sch70] Alan H. Schoen. Infinite periodic minimal surfaces without self-intersections. Technical Note D-5541, NASA, Cambridge, Mass., May 1970.
- [Tra08] Martin Traizet. On the genus of triply periodic minimal surfaces. *J. Differential Geom.*, 79(2):243–275, 2008.
- [Wey06] Adam G. Weyhaupt. *New families of embedded triply periodic minimal surfaces of genus three in euclidean space*. ProQuest LLC, Ann Arbor, MI, 2006. Thesis (Ph.D.)–Indiana University.
- [Wey08] Adam G. Weyhaupt. Deformations of the gyroid and Lidinoid minimal surfaces. *Pacific J. Math.*, 235(1):137–171, 2008.

(Chen) GEORG-AUGUST-UNIVERSITÄT GÖTTINGEN, INSTITUT FÜR NUMERISCHE UND ANGEWANDTE MATHEMATIK

E-mail address: h.chen@math.uni-goettingen.de

(Weber) INDIANA UNIVERSITY, DEPARTMENT OF MATHEMATICS

E-mail address: matweber@indiana.edu